Quantum spin-1 chains with strong planar anisotropy

1990 J. Phys.: Condens. Matter 2 6575

(http://iopscience.iop.org/0953-8984/2/31/011)

J. Phys.: Condens. Matter **2** (1990) 6575–6591. Printed in the UK

Quantum spin-1 chains with strong planar anisotropy

N Papanicolaou† and P Spathis†
Department of Physics, University of Crete, and Research Center of Crete, 714 09 Iraklion, Greece

Received 21 December 1989, in final form 5 March 1990

Abstract. Quantum spin-1 chains with strong planar anisotropy are studied using both semiclassical and strong-coupling methods. In addition to providing accurate analytical results for the dispersion and intensity of an exciton or antiexciton mode, we find that an exciton–antiexciton bound state is formed that could be observed through the two-point longitudinal dynamic correlation function which is calculated explicitly. These results are relevant for the analysis of neutron scattering experiments on $CsFeCl_3$ and $CsFeBr_3$.

1. Introduction

Quantum spin chains have long been the subject of theoretical study [1], but experimental investigations of quasi-one-dimensional magnetic systems are relatively recent [2]. With the increased popularity of this subject came an increased demand for reliable theoretical predictions. Yet the calculation of dynamic correlation functions remains difficult, even within the context of completely integrable quantum spin chains whose Hamiltonian can be diagonalised by a Bethe *ansatz* [3].

The situation is only worse for non-integrable chains, especially because the standard semiclassical theory of magnetism often fails in one dimension owing to strong quantum fluctuations. It is the purpose of this article to develop a reasonably complete theoretical framework for the class of (non-integrable) quantum spin-1 chains described by the Hamiltonian

$$H = \sum_{n=1}^{\Lambda} [A(S_n^z)^2 - J(S_n^x S_{n+1}^x + S_n^y S_{n+1}^y + \delta S_n^z S_{n+1}^z)] \tag{1.1}$$

which encompasses a number of magnetic chains of current interest. Here n is a site index, Λ is the total number of sites on a periodic chain, and the $\boldsymbol{S}_n$ are spin operators at each lattice site such that $\boldsymbol{S}_n^2 = s(s+1) = 2$. The constant A in (1.1) will be assumed

† Also at the Department of Physics, Washington University, St. Louis, MO 63130, USA.

0953-8984/90/316575 + 18 $03.50

positive, corresponding to planar anisotropy. One should also note that the transformation

$$S_n^z \to -S_n^x \qquad S_n^y \to -S_n^y \qquad S_n^z \to S_n^z$$

at alternate sites preserves the spin commutation relations while it maps the Hamiltonian (1.1) onto

$$H' = \sum_{n=1}^{\Lambda} [A(S_n^z)^2 + J(S_n^x S_{n+1}^x + S_n^y S_{n+1}^y - \delta S_n^z S_{n+1}^z)] \tag{1.2}$$

which indicates that the spectrum of the original Hamiltonian is invariant under the transformation $(J, \delta) \to (-J, -\delta)$. Therefore no loss of generality results in assuming J to be positive in (1.1). Then the isotropic ferromagnet corresponds to $A = 0$ and $\delta = 1$ and the isotropic antiferromagnet to $A = 0$ and $\delta = -1$. Nevertheless some caution is necessary in translating the above invariance of the spectrum into a corresponding statement for correlation functions. For instance, the two-point transverse correlation function calculated from the Hamiltonian (1.1) with $J > 0$ and $\delta = -1$ applies to a chain with isotropic antiferromagnetic exchange interaction, but only after a shift of the Brillouin zone is performed according to $k \to k + \pi$; no such shift is necessary for the longitudinal correlation function.

There exist at least two distinct coupling regimes controlled by the value of the dimensionless coupling constant $a = A/J$. Here we shall focus on systems realised in the strong-coupling region $a > 1$. The spectrum of the Hamiltonian (1.1) is expected to change drastically as a varies from very small to very large values. In the limit of infinite a, (1.1) reduces to a sum of single-site Hamiltonians the spectrum of which may be obtained trivially. The ground state is then the direct product of states with vanishing azimuthal spin, $S_n^z = 0$ for each site n, and has vanishing energy. Excited states can be constructed by assigning the value $S_n^z = \pm 1$ to one or more sites. The excited states fall into bands of energy A, $2A$, ..., corresponding to one, two or more sites with non-vanishing azimuthal spin of either sign. These bands are strongly degenerate in the limit of infinite a. For finite but sufficiently large a the exchange part in the Hamiltonian (1.1) may be treated as a perturbation which lifts the degeneracy and the bands acquire a finite width. We shall say that the system is realised in the strong-coupling region as long as the low-lying bands do not overlap. On the other hand, the bands are expected to overlap for sufficiently small a, a process that is eventually mediated by a phase transition at some critical value $a = a_c$. The region of present interest is $a > a_c$.

The usual semiclassical theory of magnetism is clearly inapplicable to the strong-coupling region. We have thus developed a modified semiclassical theory based on a $1/n$ expansion, which was specifically designed to account for magnetic systems with significant single-site or biquadratic interactions [4, 5]. Furthermore, in a recent short communication [6], we have shown that a direct strong-coupling expansion provides a rather efficient approach, in some respects superior to the $1/n$ expansion. In particular, we have predicted the occurrence of certain exciton–antiexciton bound states which could be observed through the two-point longitudinal dynamic correlation function.

Here we elaborate the calculation in [6] and provide explicit expressions for dynamic correlation functions. Hence in section 2 we summarise the results from the semiclassical $1/n$ expansion in order to provide a basis for comparison with the more definitive results obtained through the strong-coupling expansion in section 3. In section 4 we derive explicit expressions for the two-point transverse and longitudinal dynamic correlation

functions within the strong-coupling expansion. We show that the transverse function is dominated by elementary excitations (excitons and antiexcitons) whereas the longitudinal function is dominated by exciton–antiexciton bound states. Our conclusions are summarised in section 5.

The theoretical results presented in the paper are relevant for the analysis of quasi-one-dimensional spin-1 systems such as $CsFeCl_3$ and $CsFeBr_3$, in so far as these systems are adequately described by the simple model Hamiltonian (1.1) with $\delta = \pm 1$ and $a = 4$–5 [7–9]. However, the present authors do not have at this point explicit data for these systems; so the discussion of results from neutron scattering will be circumspect.

2. Semiclassical theory

This section surveys the essential results obtained within the $1/n$ expansion without giving calculational details [4]. We consider the two-point dynamic correlation functions at $T = 0$, namely the transverse function

$$G^{\mathrm{tr}}(k, \omega) = \frac{1}{\Lambda} \sum_{mn} \int \frac{\mathrm{d}t}{2\pi} \exp[\mathrm{i}\omega t + \mathrm{i}k(m - n)] \langle S_m^{\mu}(t) S_n^{\mu} \rangle \tag{2.1}$$

where the repeated index μ is summed over x and y, and the longitudinal function

$$G^{zz}(k, \omega) = \frac{1}{\Lambda} \sum_{mn} \int \frac{\mathrm{d}t}{2\pi} \exp[\mathrm{i}\omega t + \mathrm{i}k(m - n)] \langle S_m^{z}(t) S_n^{z} \rangle. \tag{2.2}$$

Λ is the total number of sites and the summation over m and n extends over all sites.

In the strong-coupling region the magnetisation (azimuthal spin) of the ground state vanishes ($M = 0$). Hence the transverse correlation function is dominated by elementary excitations with $M = 1$ or -1, which will be referred to as excitons or antiexcitons, respectively. An explicit calculation to leading order in the $1/n$ expansion yields

$$G^{\mathrm{tr}}(k, \omega) = 2f_k \delta(\omega - \omega_k)$$
$$\omega_k = A[1 - (4 \cos k)/a]^{1/2} \qquad f_k = [1 - (4 \cos k)/a]^{-1/2} \tag{2.3}$$

where $a = A/J$, ω_k is the energy–momentum dispersion of a doubly degenerate (anti)exciton mode and f_k determines the corresponding intensity; the factor of 2 in $2f_k$ indicates that excitons and antiexcitons contribute with equal intensity. Finally we note that the Planck constant has been set equal to unity.

For sufficiently large a the energy–momentum dispersion of equation (2.3) develops a mass gap

$$\Delta = A(1 - 4/a)^{1/2} \tag{2.4}$$

which vanishes at $a = 4$ while it becomes imaginary for $a < 4$. Thus a phase transition is predicted at the critical coupling $a = 4$ below which the doubly degenerate (anti)exciton mode bifurcates into the usual magnon and a massive resonance describing in-plane fluctuations [4]. An immediate question is whether or not the critical coupling $a = 4$ is accurate. A related concern is the accuracy of the approximate result (2.3) for values of a in the vicinity of $a = 4$, which are eventually the values of experimental interest. In fact, as is often the case with semiclassical theories, the leading $1/n$ approximation does not predict the correct critical coupling in this problem. Numerical simulations and other

evidence suggest that the true critical coupling lies in the region $a_c \simeq 1$. Therefore, for intermediate couplings in the region $a \simeq 4$, detailed numerical predictions based on equation (2.3) should be interpreted with caution.

Nevertheless the semiclassical approximation (2.3) yields a reasonable overall picture and was recently used for the analysis of neutron scattering data [8]. Actually the data were analysed on the basis of a result due to Lindgard [10], which is more general than (2.3) in that it accounts for finite temperature and a small interchain coupling. Although these effects are important for a detailed comparison with experiment, they will be neglected in the present work for simplicity. The essential physics is already present at $T = 0$, and in the absence of an interchain coupling.

On the other hand, we have challenged the accuracy of the semiclassical approximation through a direct strong-coupling expansion and found that (2.3) yields poor quantitative predictions for intermediate couplings of actual interest. Furthermore we have shown that the strong-coupling expansion yields valuable information on certain bound states that can be observed through the two-point longitudinal correlation function. A detailed discussion of these developments is given in sections 3 and 4. This section will be completed with the calculation of the longitudinal correlation function within the semiclassical approach based on the $1/n$ expansion.

To leading order we find that the two-point longitudinal function is dominated by an exciton–antiexciton continuum, namely

$$G^{zz}(k, \omega) = \int_0^{2\pi} \frac{dp}{2\pi} \delta(\omega - \omega_p - \omega_{k-p}) M(p, k-p) \tag{2.5}$$

where ω_k is the excitonic dispersion of equation (2.3), $\delta(\ldots)$ is the usual delta function and

$$M(p,q) = \tfrac{1}{2}[[1 - (2/a)(\cos p + \cos q)]/\{[1 - (4\cos p)/a][1 - (4\cos q)/a]\}^{1/2} - 1]]. \tag{2.6}$$

Although it is a relatively straightforward matter to perform the integration in (2.5) numerically, the essential features of this result become apparent in the strong-coupling region, $a \gg 1$, where

$$\omega_k \simeq A[1 - (2\cos k)/a] \qquad M(p, q) \simeq (1/a^2)(\cos p - \cos q)^2 \tag{2.7}$$

and the integration in (2.5) can be done analytically:

$$G^{zz}(k, \omega) \simeq (1/2\pi aA) \tan^2(k/2) [4\cos^2(k/2) - a^2(1 - \omega/2A)^2]^{1/2}. \tag{2.8}$$

Viewing $G^{zz}(k, \omega)$ as a function of frequency ω at fixed momentum k, equation (2.8) yields a non-vanishing result over a finite interval determined by the requirement that the argument under the square root be positive. The correlation function vanishes outside that interval.

The longitudinal correlation function calculated above is a dull function of frequency, symmetric around $\omega = 2A$, and provides no indication for a sharp mode in this channel. In particular, this semiclassical result cannot account for a certain mirror mode picked up by out-of-plane fluctuations in the experiment in [8]. However, as we shall see in the following sections, a calculation within the strong-coupling expansion gives an expression for $G^{zz}(k, \omega)$ that contains a contribution from a sharp exciton–antiexciton bound state.

Finally we note that both the transverse function in equation (2.3) and the longitudinal function in equation (2.8) are independent of the strength δ of the Ising term in

the Hamiltonian (1.1). Such a result appears reasonable to leading order, because out-of-plane fluctuations are suppressed for large values of a, but some dependence on δ should be expected in higher-order corrections to (2.3) and (2.8). In fact the direct strong-coupling expansion will confirm the above picture to a large extent for the transverse correlation function, but not for the longitudinal function for which the Ising term will prove to be important even to leading order.

3. Strong-coupling expansion

In order to elucidate the issues raised in the preceding sections we have carried out a strong-coupling expansion for the low-lying spectrum of the Hamiltonian (1.1) and the corresponding dynamic correlation functions. In this section we present explicit results for the ground state, exciton and antiexciton states, as well as exciton–exciton, anti-exciton–antiexciton and exciton–antiexciton bound states. The calculation of dynamic correlation functions is relegated to section 4.

To carry out the strong-coupling expansion the Hamiltonian (1.1) is written as

$$H/A = H_0 - (1/a)V$$

$$H_0 = \sum_{n=1}^{\Lambda} (S_n^z)^2 \qquad V = \sum_{n=1}^{\Lambda} [\tfrac{1}{2}(S_n^+ S_{n+1}^- + S_n^+ S_{n-1}^-) + \delta S_n^z S_{n+1}^z] \tag{3.1}$$

where H_0 is treated as the zeroth-order Hamiltonian, whereas the term $(-1/a)V$ is treated as a small perturbation within a systematic expansion in inverse powers of a.

The spectrum of H_0 is constructed trivially and has already been described in section 1. Thus the zeroth-order ground state is given simply by $|0\rangle = |0, 0, \ldots, 0\rangle$, which is the state with all sites carrying vanishing azimuthal spin and has vanishing energy. This state is non-degenerate, so the calculation of higher-order corrections is relatively straightforward. Including the first-order correction the ground state is given by

$$|\Omega\rangle = |0\rangle + \frac{1}{2a}\sum_n [|n, \overline{n+1}\rangle + |\bar{n}, n+1\rangle] + O\left(\frac{1}{a^2}\right) \tag{3.2}$$

where $|n_1, \bar{n}_2\rangle$ denotes a state with sites n_1 and n_2 carrying azimuthal spin equal to $+1$ and -1, respectively, while the azimuthal spin vanishes at all other sites. The calculation of the ground state was actually carried through to fourth order. We quote here the final result for the ground-state energy;

$$\begin{aligned} &E_{gr}/A\Lambda = \varepsilon_0 + \varepsilon_1/a + \varepsilon_2/a^2 + \varepsilon_3/a^3 + \varepsilon_4/a^4 + \ldots \\ &\varepsilon_0 = 0 = \varepsilon_1 \qquad \varepsilon_2 = -1 \qquad \varepsilon_3 = \delta/2 \qquad \varepsilon_4 = (2 - \delta^2)/4. \end{aligned} \tag{3.3}$$

Note that the first few terms in (3.3) are δ independent, in accord with our earlier remark that out-of-plane fluctuations tend to be suppressed in the limit of large a.

Next we consider the manifold of states of the form $|n\rangle$ or $|\bar{n}\rangle$ where only the site n carries non-vanishing azimuthal spin equal to $+1$ or -1, respectively. There exist Λ states of type $|n\rangle$, with $n = 1, 2, \ldots, \Lambda$, which will be called excitons (e), and Λ states of type $|\bar{n}\rangle$ which will be called antiexcitons ($\bar{e}$). Both $|n\rangle$ and $|\bar{n}\rangle$ are eigenstates of the

zeroth-order Hamiltonian with energy equal to A for any n. This degeneracy is removed by constructing states with definite crystal momentum:

$$|k\rangle = \frac{1}{\sqrt{\Lambda}} \sum_n \exp(ikn)\,|n\rangle \qquad |\bar{k}\rangle = \frac{1}{\sqrt{\Lambda}} \sum_n \exp(ikn)\,|\bar{n}\rangle. \tag{3.4}$$

For any given value of crystal momentum k and magnetisation $M = \pm 1$, the zeroth-order states (3.4) are non-degenerate and higher-order corrections are again obtained through non-degenerate perturbation theory. Hence, to leading order, the one-exciton state is given by

$$|\Psi_k\rangle = |k\rangle + \frac{1}{2a\sqrt{\Lambda}} \sum_n \exp(ikn) \left(2\cos k\,|n+1, \bar{n}, n-1\rangle + \sum_{\substack{m \\ (m \neq n, n\pm 1)}} (|m, \overline{m+1}, n\rangle + |\bar{m}, m+1, n\rangle) \right) + O\left(\frac{1}{a^2}\right) \tag{3.5a}$$

and the one-antiexciton state by

$$|\bar{\Psi}_k\rangle = |\bar{k}\rangle + \frac{1}{2a\sqrt{\Lambda}} \sum_n \exp(ikn) \left(2\cos k\,|\overline{n+1}, n, \overline{n-1}\rangle + \sum_{\substack{m \\ (m \neq n, n\pm 1)}} (|m, \overline{m+1}, \bar{n}\rangle + |\bar{m}, m+1, \bar{n}\rangle) \right) + O\left(\frac{1}{a^2}\right) \tag{3.5b}$$

where we use a straightforward generalisation of notation introduced earlier. The calculation was actually carried through to third order. We quote here an explicit third-order expression for the excitation energy of exciton or antiexciton states, namely

$$\begin{aligned} \omega_k &= A(1 + \omega_1/a + \omega_2/a^2 + \omega_3/a^3 + \ldots) \\ \omega_1 &= -2\cos k \qquad \omega_2 = 1 + 2\sin^2 k \\ \omega_3 &= \tfrac{1}{2}(1 + 8\sin^2 k)\cos k - 2\delta \sin^2 k. \end{aligned} \tag{3.6}$$

Note again that the first few terms in (3.6) are δ independent.

We are now in a position to make a first comparison with the semiclassical results in section 2. In figure 1 we compare the strong-coupling approximation (3.6) with the semiclassical approximation (2.3) for a typical large coupling $a = 10$. The dispersion is depicted for both ferromagnetic ($\delta = 1$) and antiferromagnetic ($\delta = -1$) exchange interaction, having incorporated the shift $k \rightarrow k + \pi$ in the latter case. The observed discrepancy between the two curves arises because the semiclassical result (2.3) is only the leading approximation within the $1/n$ expansion, whereas the strong-coupling series (3.6) was carried to third order and yields a rapidly converging sequence for $a = 10$. Therefore it is almost certain that (3.6) gives an excellent approximation in this region of couplings while a comparable accuracy would be achieved within the semiclassical theory by calculating higher-order $1/n$ corrections.

To simplify the picture we consider the mass gap calculated from the strong-coupling series (3.6):

$$\Delta = \omega_{k=0} = A(1 - 2/a + 1/a^2 + 1/2a^3 + \ldots) \tag{3.7}$$

and compare it with the leading-order semiclassical result in equation (2.4). It is clear

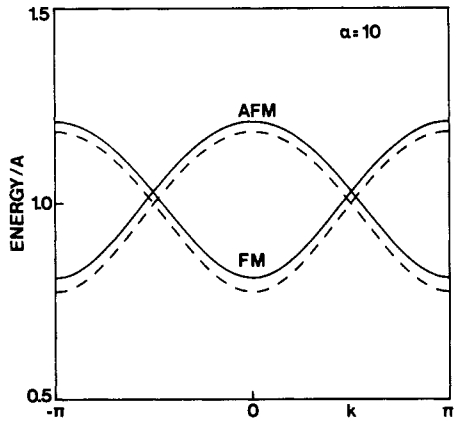

Figure 1. Energy–momentum dispersion of the (anti)exciton mode for a typical strong anisotropy ($a = 10$). The dispersion is plotted for both ferromagnetic (FM) and antiferromagnetic (AFM) exchange interaction. The full curves depict the result of the strong-coupling expansion, (3.6), and the broken curves correspond to the semiclassical result (2.3).

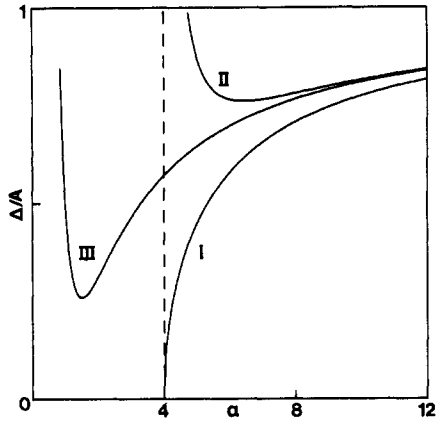

Figure 2. Mass gap as a function of a; curve I depicts the leading-order semiclassical approximation (2.4), curve II includes the first (anharmonic) $1/n$ correction to (2.4), and curve III is the strong-coupling approximation of (3.7).

that, for very large values of a, equations (2.4) and (3.7) can both be approximated by $\Delta \simeq A(1 - 2/a)$ and thus coincide. Significant deviations begin to emerge at, say, $a \simeq 10$, as is apparent in figure 2 which depicts the mass gap as a function of a. As expected, the discrepancy is reduced by including the first (anharmonic) $1/n$ correction to equation (2.4), which was calculated in [4] and is also shown in figure 2.

Nonetheless the picture becomes more subtle for the intermediate couplings of actual interest. For $a \simeq 4$, the last term in equation (3.7) contributes only a few per cent of the total value, which makes it reasonable to assume that the strong-coupling series remains reliable in this region of couplings yielding an estimate of $\Delta \simeq 0.57A$ for the mass gap at $a_c = 4$. On the other hand, the leading-order semiclassical result (2.4) yields a vanishing mass gap at $a = 4$, while the first anharmonic correction shown in figure 2 becomes divergent. This singular behaviour reflects the fact that the semiclassical critical coupling $a = 4$ is inaccurate. Hence the semiclassical theory cannot be useful in the region $a \simeq 4$, unless tedious resummation techniques are invoked.

Therefore the strong-coupling series (3.6) yields a more reliable description of the (anti)exciton mode for strong as well as intermediate couplings. Furthermore pushing the calculation to high orders would help to locate the true critical coupling and to elucidate the nature of the phase transition. The first few terms in equation (3.7) already suggest that the critical coupling should lie in the region $a \simeq 1$. The high-order behaviour of this series is expected to be especially interesting in view of the anticipated Haldane gap at $a = 0$ and $\delta = -1$ and the absence of a gap at $a = 0$ and $\delta = 1$. Note that the first few terms displayed in equation (3.7) are δ independent, but this situation is expected to change in higher-order terms.

The practical outcome of the preceding discussion is that neutron scattering data should be reanalysed in the light of equation (3.6). Here we consider briefly the (anti)exciton dispersion of $CsFeBr_3$ for which [8] assigns the parameters $\delta = -1$, $A =$

29.8 K, $J = 6.4$ K ($a = A/J = 4.7$), which have been adapted to our current conventions. These parameters were extracted essentially from a fit of the data against the semiclassical dispersion of equation (2.3). We thus use equation (2.3) with the above parameters as input 'experimental' data and perform a least-squares fit to the dispersion (3.6). Assuming that $\delta = -1$, the resulting new parameters $A = 23$ K, $J = 7$ K ($a = A/J = 3.3$) are found in substantial disagreement with the original assignment. The most notable feature of the new parameters is that the value of a is pushed below the semiclassical critical coupling $a_c = 4$, where equation (2.3) is no longer valid. Needless to say, a more careful analysis should use equation (3.6) in conjunction with actual data and include the effect of a small interchain coupling. Finally the energy–momentum dispersion (3.6) must be completed with an explicit expression for the intensity of the excitonic mode, which will be given in section 4 of the present paper.

Having thus completed the description of excitons and antiexcitons, we turn our attention to two-body states, namely exciton–exciton (ee) pairs with magnetisation $M = 2$, antiexciton–antiexciton ($\bar{e}\bar{e}$) pairs with $M = -2$, and exciton–antiexciton ($e\bar{e}$) pairs with $M = 0$. The ee and $\bar{e}\bar{e}$ states share with more conventional two-magnon states the property that they may be observed only through four-point correlations. In contrast, $e\bar{e}$ states contribute directly to the two-point longitudinal dynamic correlation function, because they carry the same magnetisation as the ground state ($M = 0$), and should be accessible to inelastic neutron scattering. It is thus important to examine whether bound states can be formed, which could then be observed by neutron scattering through out-of-plane fluctuations.

The leading-order semiclassical calculation in section 2 failed to provide evidence for the formation of bound states, for more or less the same reason that the familiar Holstein–Primakoff theory does not yield direct information for the two-magnon bound states known to occur in ferromagnets. Therefore, to ascertain the existence of bound states in the present problem, we resort again to the strong-coupling expansion.

We analyse first the ee sector. In the limit $a \to \infty$, this sector consists of states of the form $|n_1, n_2\rangle$ where the azimuthal spin is equal to $+1$ at sites n_1 and n_2 and vanishes at all other sites. Since $n_1 \neq n_2$ and $|n_1, n_2\rangle = |n_2, n_1\rangle$, there exist $\Lambda(\Lambda - 1)/2$ ee states all with energy $2A$. Such a strong degeneracy cannot be completely removed by sorting out states with definite crystal momentum. Hence we must perform degenerate perturbation theory; to leading order, we must diagonalise the matrix $\langle n_1', n_2'|V|n_1, n_2\rangle$ where V is the exchange operator defined in equation (3.1). The action of V on $|n_1, n_2\rangle$ is given by

$$V|n_1, n_2\rangle = |n_1 - 1, n_2\rangle + |n_1 + 1, n_2\rangle + |n_1, n_2 - 1\rangle + |n_1, n_2 + 1\rangle \tag{3.8a}$$

when n_1 and n_2 are not neighbours, and

$$V|n, n+1\rangle = \delta|n, n+1\rangle + |n-1, n+1\rangle + |n, n+2\rangle. \tag{3.8b}$$

In the right-hand sides of equations (3.8*a*) and (3.8*b*) we have omitted states that contain more or less than two sites with non-vanishing azimuthal spin, as is appropriate to leading order.

The main point of this calculation is that the operator V defined by equation (3.8) can be diagonalised by an elementary Bethe *ansatz*, in close analogy with calculations of two-magnon states in anisotropic chains of arbitrary spin [11, 12]. Thus we consider the eigenvalue problem

$$V|\psi\rangle = \varepsilon|\psi\rangle \qquad |\psi\rangle = \sum_{n_1<n_2} C_{n_1,n_2}|n_1, n_2\rangle. \tag{3.9}$$

In view of equation (3.8) the coefficients C_{n_1,n_2} satisfy the system of linear equations

$$\varepsilon C_{n_1,n_2} = C_{n_1-1,n_2} + C_{n_1+1,n_2} + C_{n_1,n_2+1} + C_{n_1,n_2-1} \qquad \text{for } n_1 < n_2 - 1$$
$$\varepsilon C_{n,n+1} = \delta C_{n,n+1} + C_{n-1,n+1} + C_{n,n+2}. \tag{3.10}$$

This system is solved by the Bethe *ansatz*

$$C_{n_1,n_2} = \exp[\mathrm{i}(k_1 n_1 + k_2 n_2 + \varphi/2)] + \exp[\mathrm{i}(k_1 n_2 + k_2 n_1 - \varphi/2)]$$
$$\varepsilon = 2(\cos k_1 + \cos k_2) \tag{3.11}$$

provided that the wavenumbers k_1, k_2 and the phase shift φ are related by

$$\cot(\varphi/2) = \{\delta \sin[(k_1 - k_2)/2]\}/\{2\cos[(k_1 + k_2)/2] - \delta \cos[(k_1 - k_2)/2]\}. \tag{3.12}$$

The wavenumbers and the phase shift are further constrained by the periodic boundary condition

$$C_{n_1,n_2} = C_{n_2,n_1+\Lambda} \tag{3.13}$$

which leads to the relations

$$\Lambda k_1 - \varphi = 2\pi\lambda_1 \qquad \Lambda k_2 + \varphi = 2\pi\lambda_2 \tag{3.14}$$

where λ_1 and λ_2 are integers such that

$$0 \leqslant \lambda_1 \leqslant \lambda_2 \leqslant \Lambda - 1. \tag{3.15}$$

Finally the leading approximation to the excitation energy of an ee pair is given by $\Omega_{k_1k_2} \simeq A(2 - \varepsilon/a)$, or

$$\Omega_{k_1k_2} = 2A[1 - (1/a)(\cos k_1 + \cos k_2)]. \tag{3.16}$$

We have thus summarised all information necessary for a complete analysis of the ee sector along the lines of [11, 12]. For any set of integers λ_1 and λ_2 in the range (3.15), equations (3.11), (3.12) and (3.14) provide a solution of the eigenvalue problem (3.9). There exist essentially two categories of solutions corresponding to $\lambda_1 < \lambda_2 - 1$, and $\lambda_1 = \lambda_2$ or $\lambda_1 = \lambda_2 - 1$. The majority of solutions belong in the first category and yield real wavenumbers k_1 and k_2. The excitation energies of these solutions fall into a two-body continuum given by the eigenvalues (3.16) parametrised in terms of the total crystal momentum $k = k_1 + k_2 (\mathrm{mod}\, 2\pi)$. After a proper folding of the wavevector $k = k_1 + k_2$ to the first Brillouin zone, the continuum extends between the two boundaries

$$\Omega_k^{\pm} = 2A[1 \pm (2/a)\cos(k/2)]. \tag{3.17}$$

The second category of solutions, with $\lambda_1 = \lambda_2$ or $\lambda_1 = \lambda_2 - 1$, may lead to complex wavenumbers of the form $k_1 = u + \mathrm{i}v$ and $k_2 = u - \mathrm{i}v$. Equation (3.14) then yields $\varphi = \mathrm{i}\Lambda v$ for $\lambda_1 = \lambda_2$ or $\varphi = \mathrm{i}\Lambda v + \pi$ for $\lambda_1 = \lambda_2 - 1$. Substituting these relations in equation (3.12) and taking the thermodynamic limit ($\Lambda \to \infty$) we find that

$$2\cos u = \delta \exp(-v) \qquad u = (k_1 + k_2)/2 = k/2 \qquad v = (k_1 - k_2)/2\mathrm{i} \tag{3.18}$$

where v is assumed positive, negative v leading to identical results. The excitation energy calculated by inserting (3.18) into (3.16) is denoted by Ω_k^{ee}:

$$\Omega_k^{\mathrm{ee}} = 2A\{1 - (1/a)[\delta/2 + (2/\delta)\cos^2(k/2)]\}. \tag{3.19}$$

A further consequence of equation (3.18) is that complex solutions exist only when

$0 \leqslant \cos(k/2) \leqslant \delta/2$ for $\delta > 0$, or $0 \geqslant \cos(k/2) \geqslant \delta/2$ for $\delta < 0$. The usual folding of the zone leads to the single condition

$$k_0 \leqslant |k| \leqslant \pi \qquad k_0 = 2\cos^{-1}(|\delta|/2) \tag{3.20}$$

where k is the crystal momentum appearing in equation (3.19) and is defined in the first Brillouin zone.

A solution with complex wavenumbers describes a bound state of two excitons, with energy–momentum dispersion given by equation (3.19). The dispersion lies below the continuum for $\delta > 0$ and above the continuum for $\delta < 0$. In both cases the dispersion merges with the continuum at the cut-off momentum $|k| = k_0 = 2\cos^{-1}(|\delta|/2)$ below which the bound state is unstable. Note that the bound state is stable throughout the zone for $|\delta| > 2$, whereas no such state is possible in the XY limit $\delta = 0$.

The description of the $\bar{e}\bar{e}$ sector is completely analogous and leads to a bound state with the same dispersion as in equation (3.19). We thus turn our attention to the exciton–antiexciton ($e\bar{e}$) sector which is crucial for the calculation of the longitudinal dynamic correlation function. In the strong-coupling limit, $a \to \infty$, the $e\bar{e}$ sector is spanned by states of the form $|n_1, \bar{n}_2\rangle$ where the bar indicates that the azimuthal spin at site n_2 is equal to -1. The study of this sector appears to be complicated by the fact that $|n_1, \bar{n}_2\rangle$ is not symmetric under exchange of n_1 and n_2. Nevertheless it is not difficult to see that the (anti)symmetric combinations

$$|n_1, n_2\rangle^{\pm} = (1/\sqrt{2})[|n_1, \bar{n}_2\rangle \pm |n_2, \bar{n}_1\rangle] \tag{3.21}$$

both satisfy equation (3.8) with the simple substitution $\delta \to -\delta$. Therefore the corresponding eigenvalue problem is solved by wavefunctions of the form

$$|\psi\rangle^{\pm} = \sum_{n_1 < n_2} C_{n_1, n_2} |n_1, n_2\rangle^{\pm} \tag{3.22}$$

where the coefficients are again given by equation (3.11), except that the wavenumbers and the phase shift are now related by

$$\cot(\varphi/2) = \{-\delta \sin[(k_1 - k_2)/2]\}/\{2\cos[(k_1 + k_2)/2] + \delta \cos[(k_1 - k_2)/2]\} \tag{3.23}$$

which differs from equation (3.12) in the sign of δ. A difference arises also in the periodic boundary condition which should read

$$C_{n_1, n_2} = C_{n_2, n_1 + \Lambda} \quad \text{or} \quad C_{n_1, n_2} = -C_{n_2, n_1 + \Lambda} \tag{3.24}$$

for the symmetric or antisymmetric combinations in equation (3.22), respectively. Expressing these conditions in terms of the wavenumbers and the phase shift leads to equation (3.14) in both cases, but the λ_1 and λ_2 are integers in the first case and half-integers in the second. Nonetheless, in the thermodynamic limit, the dispersions for the $e\bar{e}$ bound state are found to be the same for both cases in (3.24), namely

$$\Omega_k^{e\bar{e}} = 2A\{1 + (1/a)[\delta/2 + (2/\delta)\cos^2(k/2)]\} \tag{3.25}$$

which differs from equation (3.19) only in the sign of δ. On the other hand, the boundaries of the $e\bar{e}$ continuum are the same with those of the ee or $\bar{e}\bar{e}$ continuum given in equation (3.17). Hence the $e\bar{e}$ dispersion (3.25) emerges above the continuum for $\delta > 0$ and below the continuum for $\delta < 0$; no bound state occurs in the XY limit $\delta = 0$.

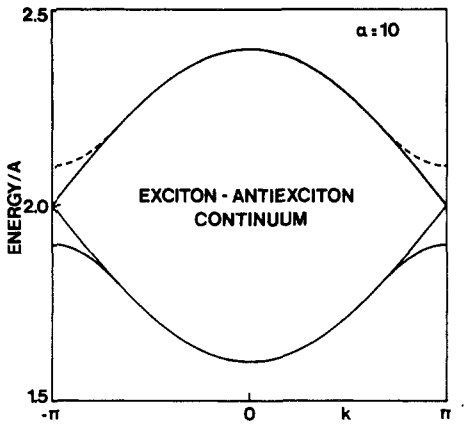

Figure 3. Excitation spectrum of exciton–antiexciton ($e\bar{e}$) states for a typical strong coupling ($a = 10$). The bound state emerges below the continuum for the antiferromagnet (full curve, $\delta = -1$) and above the continuum for the ferromagnet (broken curve, $\delta = 1$).

The above result is illustrated in figure 3 for a typical strong coupling $a = 10$ and ferromagnetic ($\delta = 1$) as well as antiferromagnetic ($\delta = -1$) exchange interaction. The physical characteristics of the $e\bar{e}$ bound state will become apparent through its contribution to $G^{zz}(k, \omega)$ which is calculated explicitly in the following section.

4. Dynamic correlation functions

The results of the previous section are best summarised with an explicit calculation of the two-point dynamic correlation functions at $T = 0$. We begin with the transverse function defined in equation (2.1). After taking the usual steps of inserting a complete set of states, and making the time dependence explicit using the evolution operator $\exp(-iHt)$, we obtain

$$G^{tr}(k, \omega) = \frac{1}{\Lambda} \sum_{mn} \exp[ik(m-n)] \sum_{\gamma} \langle \Omega | S_m^{\mu} | \gamma \rangle \langle \gamma | S_n^{\mu} | \Omega \rangle \delta(\omega - \omega_{\gamma}) \tag{4.1}$$

where μ is summed over x and y, $|\Omega\rangle$ is the ground state, and the sum over γ extends over a complete set of eigenstates $|\gamma\rangle$ with eigenvalues ω_{γ}. Since the magnetisation of the ground state vanishes ($M = 0$), it is clear that only states with $M = \pm 1$ contribute to this sum. The dominant contribution arises from single exciton or antiexciton states. There are also contributions from higher bands with $M = \pm 1$, such as $ee\bar{e}$ or $e\bar{e}\bar{e}$, but a discussion of these effects is deferred for the moment.

Thus we proceed to calculate the contribution of excitons and antiexcitons to the sum of equation (4.1). The relevant non-vanishing amplitudes are

$$\langle \Omega | S_n^- | \psi_k \rangle \quad \text{and} \quad \langle \Omega | S_n^+ | \bar{\psi}_k \rangle$$

where $|\Omega\rangle$ is the ground state (3.2), while $|\psi_k\rangle$ and $|\bar{\psi}_k\rangle$ are the exciton and antiexciton eigenstates of equation (3.5). A second-order calculation yields

$$\langle \Omega | S_n^- | \psi_k \rangle = \langle \Omega | S_n^+ | \bar{\psi}_k \rangle = (2/\Lambda)^{1/2} \exp(ikn)[1 + (1/a)\cos k + (1/4a^2) \times (10\cos^2 k - 2\delta \cos k - 7) + O(1/a^3)] \tag{4.2}$$

which is then used in equation (4.1) to obtain

$$G^{tr}(k, \omega) = 2f_k \delta(\omega - \omega_k)$$
$$f_k = 1 + (2/a)\cos k + (1/2a^2)(12\cos^2 k - 2\delta \cos k - 7) + O(1/a^3) \tag{4.3}$$

where ω_k is the (anti)exciton dispersion given earlier in equation (3.6). The amplitude f_k may be used to calculate the intensity of exciton and antiexciton modes.

Comparing the above result with its semiclassical analogue in equation (2.3) we see that agreement obtains for very large values of a for which $\omega_k \simeq A[1 - (2\cos k)/a]$ and $f_k \simeq 1 + (2\cos k)/a$ in both cases. For intermediate values of a, (4.3) is superior to (2.3) for reasons already explained in section 3. Nevertheless one should keep in mind that equation (4.3) is approximate in two ways. First, it is based on a strong-coupling expansion which could, in principle, be improved further by calculating higher-order corrections. Second, we have neglected in equation (4.1) contributions from higher $M = \pm 1$ bands such as $ee\bar{e}$, $e\bar{e}\bar{e}$ and so on. Yet, for sufficiently strong anisotropy, these bands are widely separated from the fundamental e or $\bar{e}$ band and can be safely ignored. As a consequence, the (anti)exciton mode appears as a sharp δ-function peak in the transverse correlation function. This situation has been confirmed in $CsFeCl_3$ and $CsFeBr_3$ where the observed modes are sharp to within experimental resolution [7–9]. Of course, the various bands will begin to overlap for sufficiently small a, in the region $a \simeq 1$, and the (anti)exciton mode will acquire a finite width. For even smaller values of a, a description in terms of (anti)excitons is no longer valid and the system undergoes a phase transition.

Our discussion of the transverse correlation function is completed here with a reminder concerning the choice of the parameter δ. As long as the exchange constant J is kept positive in equation (1.1), equations (3.6) and (4.3) apply to a chain with isotropic ferromagnetic exchange interaction simply by setting $\delta = 1$. The corresponding results for a chain with isotropic antiferromagnetic exchange interaction were obtained by setting $\delta = -1$ in equations (3.6) and (4.3) and by shifting the Brillouin zone according to $k \to k + \pi$. This procedure was already followed in figure 1. To be sure, the dispersion ω_k and the amplitude f_k are then given by

$$\omega_k = A\{1 + (2/a)\cos k + (1/a^2)(1 + 2\sin^2 k) + (1/a^3)[2\sin^2 k - \tfrac{1}{2}(1 + 8\sin^2 k)\cos k] + O(1/a^4)\} \tag{4.4}$$

$$f_k = 1 - (2/a)\cos k + (1/2a^2)(12\cos^2 k - 2\cos k - 7) + O(1/a^3)$$

and are relevant for the analysis of $CsFeBr_3$ as long as the interchain coupling can be neglected [8].

The two-point longitudinal function may be written in a form analogous to equation (4.1):

$$G^{zz}(k, \omega) = \frac{1}{\Lambda}\sum_{mn} \exp[ik(m-n)] \sum_{\gamma} \langle\Omega|S_m^z|\gamma\rangle\langle\gamma|S_n^z|\Omega\rangle \delta(\omega - \omega_\gamma) \tag{4.5}$$

where the sum over γ extends over all eigenstates with magnetisation $M = 0$. The first non-vanishing contribution to this sum emerges from the $e\bar{e}$ eigenstates constructed in section 3. There are also contributions from higher $M = 0$ bands, such as $ee\bar{e}\bar{e}$, but those may be neglected in the strong-coupling limit for reasons explained earlier in this section.

Hence our immediate task is to calculate matrix elements of the form

$$\langle\Omega|S_n^z|\psi\rangle^{\pm} \tag{4.6}$$

where $|\Omega\rangle$ is the ground state of equation (3.2) and $|\psi\rangle^{\pm}$ are the $e\bar{e}$ eigenstates of equation (3.22). To leading order, we find that

$$S_n^z|\Omega\rangle = (1/2a)[(|n, \overline{n+1}\rangle - |\bar{n}, n+1\rangle) - (|n-1, \bar{n}\rangle - |\overline{n-1}, n\rangle)]$$
$$= (1/a\sqrt{2})(|n, n+1\rangle^- - |n-1, n\rangle^-). \tag{4.7}$$

In the second step of equation (4.7) we have invoked the abbreviated notation of

equation (3.21). Also using the general form of the e$\bar{\text{e}}$ eigenstate given in equation (3.22) we find that

$$\begin{aligned}\langle\Omega|S_n^z|\psi\rangle^+ &= 0\\ \langle\Omega|S_n^z|\psi\rangle^- &= (1/\sqrt{2}\,aN)(C_{n,n+1} - C_{n-1,n})\end{aligned} \tag{4.8}$$

where N is the norm of the e$\bar{\text{e}}$ eigenstate, which was omitted in the discussion in section 3.

The leading-order contribution to equation (4.5) is now calculated by restricting the sum to states of the form $|\gamma\rangle = |\psi\rangle^-$ and by using equation (4.8) to furnish the necessary matrix elements. The sum over γ is then replaced by

$$\frac{1}{2a^2}\sum_{\lambda_1\lambda_2}\frac{1}{N^2}(C_{m,m+1} - C_{m-1,m})(C^*_{n,n+1} - C^*_{n-1,n})\delta(\omega - \Omega^{e\bar{e}}) \tag{4.9}$$

where the coefficients C_{n_1,n_2} are given by the Bethe *ansatz* (3.11), with wavenumbers k_1, k_2 and phase shift φ related by equation (3.23), N is the norm of the e$\bar{\text{e}}$ eigenstate and $\Omega^{e\bar{e}}$ are the e$\bar{\text{e}}$ eigenvalues. One should take into account that all of these quantities are eventually functions of the wavenumbers λ_1 and λ_2 introduced in equation (3.14), which take half-integer values, in the interval $0 \leqslant \lambda_1 \leqslant \lambda_2 \leqslant \Lambda - 1$, because the only e$\bar{\text{e}}$ states that contribute to (4.9) are those with negative exchange parity. Finally the sum in equation (4.9) should distinguish between scattering and bound e$\bar{\text{e}}$ eigenstates, in accord with our analysis in section 3.

Thus we have sketched the calculation of the longitudinal function to leading order in the strong-coupling expansion. The actual calculation is somewhat lengthy; so we quote only the final result:

$$G^{zz}(k,\omega) = C_1(k)\theta(|k| - k_0)\delta(\omega - \Omega_k^{e\bar{e}}) + C_2(k,\omega). \tag{4.10a}$$

The contribution of the bound state is represented by the first term in the right-hand side of equation (4.10*a*), where $\delta(\omega - \Omega_k^{e\bar{e}})$ is the usual delta function, $\Omega_k^{e\bar{e}}$ being the energy of the e$\bar{\text{e}}$ bound state;

$$\Omega_k^{e\bar{e}} = 2A\{1 + (1/a)[\delta/2 + (2/\delta)\cos^2(k/2)]\} \tag{4.10b}$$

and $\theta(|k| - k_0)$ is a step function, such that $\theta(x > 0) = 1$ and $\theta(x < 0) = 0$, where k_0 is the cut-off crystal momentum at which the bound state merges with the continuum:

$$k_0 = 2\cos^{-1}(|\delta|/2). \tag{4.10c}$$

The amplitude C_1 is given by

$$C_1(k) = \{[2\sin^2(k/2)]/a^2\delta^2\}[\delta^2 - 4\cos^2(k/2)] \tag{4.10d}$$

and is the weight of the bound state. Note that C_1 is positive for $|k| > k_0$ and vanishes at the cut-off momentum k_0. Finally the contribution of the e$\bar{\text{e}}$ continuum is represented by the last term in (4.10*a*), namely

$$\begin{aligned}C_2(k,\omega) = (1/2\pi aA)\{&\sin^2(k/2)/[\cos^2(k/2) + a(\delta/2)(1 - \omega/2A) + (\delta/2)^2]\}\\ &\times [4\cos^2(k/2) - a^2(1 - \omega/2A)^2]^{1/2}\end{aligned} \tag{4.10e}$$

and takes non-vanishing values over the finite frequency interval

$$\Omega_k^- \leqslant \omega \leqslant \Omega_k^+ \qquad \Omega_k^\pm = 2A[1 \pm (2/a)\cos(k/2)] \tag{4.10f}$$

where $\Omega_k^\pm$ are the boundaries of the continuum.

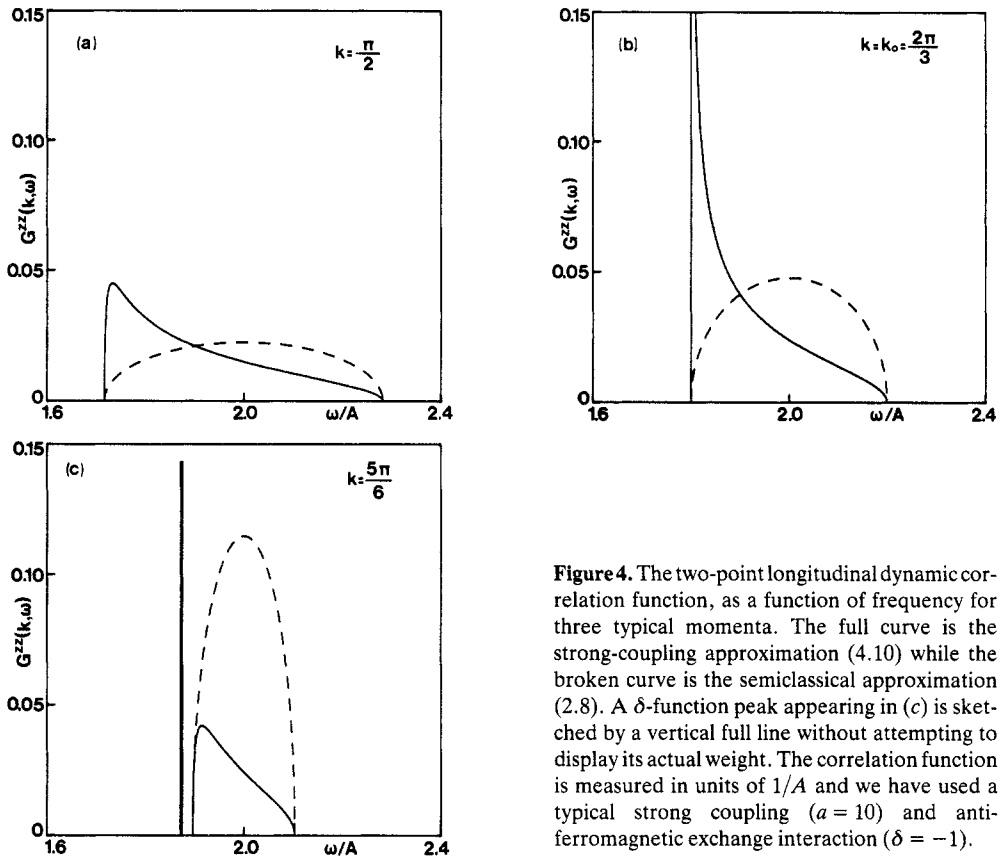

Figure 4. The two-point longitudinal dynamic correlation function, as a function of frequency for three typical momenta. The full curve is the strong-coupling approximation (4.10) while the broken curve is the semiclassical approximation (2.8). A δ-function peak appearing in (*c*) is sketched by a vertical full line without attempting to display its actual weight. The correlation function is measured in units of $1/A$ and we have used a typical strong coupling ($a = 10$) and antiferromagnetic exchange interaction ($\delta = -1$).

The above result is illustrated in figure 4 for a typical strong coupling ($a = 10$) and antiferromagnetic exchange interaction ($\delta = -1$). The cut-off momentum is then given by $k_0 = 2\pi/3$. We thus plot $G^{zz}(k, \omega)$ as a function of frequency ω for three typical values of crystal momentum k: in figure 4(*a*) for $k = \pi/2 < k_0$, for which no bound state is possible, and so the correlation function (4.10) does not contain a δ-function but exhibits a broader peak at

$$\omega = \Omega_k^{\max} = 2A[\![1 + (2\delta/a)\{\cos^2(k/2)/[\cos^2(k/2) + (\delta/2)^2]\}]\!] \qquad (4.11)$$

foreshadowing the appearance of a bound state for momenta near the zone boundary; in figure 4(*b*) for $k = 2\pi/3 = k_0$, for which the peak of the correlation function develops into a square-root singularity at the lower edge of the continuum; in figure 4(*c*) for $k = 5\pi/6 > k_0$, for which a δ-function peak does indeed emerge below the continuum.

Figure 4 also contains a comparison of equations (4.10) with the semiclassical analogue in equation (2.8). The latter exhibits a broad peak at around $\omega = 2A$ for all values of crystal momentum. The main difference is, of course, the absence of a bound state in the semiclassical result. A closer comparison reveals that equation (2.8) is the $\delta = 0$ limit of equations (4.10). In other words, agreement obtains only in the XY limit. Putting it differently, the leading-order semiclassical result unduly suppresses out-of-plane fluctuations, thus missing important information about the e$\bar{\text{e}}$ bound state. Nevertheless

we shall see shortly that the total intensity computed from equations (4.10) is δ independent and thus coincides with the intensity computed from equation (2.8).

In order to compute the total intensity, and also to appreciate the relative weight of the $e\bar{e}$ bound state, we integrate both sides of equation (4.10*a*) over all frequencies:

$$\int_0^\infty d\omega\, G^{zz}(k, \omega) = W_1(k) + W_2(k) \tag{4.12}$$

where $W_1(k)$, the weight of the bound state, is

$$W_1(k) = \begin{cases} C_1(k) = \{[2\sin^2(k/2)]/a^2\delta^2\}[\delta^2 - 4\cos^2(k/2)] & \text{for } |k| > k_0 \\ 0 & \text{for } |k| < k_0 \end{cases} \tag{4.13}$$

and $W_2(k)$, the weight of the continuum, is

$$W_2(k) = \int_0^\infty d\omega\, C_2(k,\omega) = \begin{cases} (2\sin^2 k)/a^2\delta^2 & \text{for } |k| > k_0 \\ [2\sin^2(k/2)]/a^2 & \text{for } |k| < k_0. \end{cases} \tag{4.14}$$

The total weight is then given by

$$\int_0^\infty d\omega\, G^{zz}(k, \omega) = \frac{2\sin^2(k/2)}{a^2} \tag{4.15}$$

for all values of k, above or below the cut-off momentum k_0. Thus we see that the total weight vanishes at the zone centre and attains its maximum value at the zone boundary. For $|k| < k_0$ the total weight is absorbed by the continuum while for $|k| > k_0$ it is distributed between the bound state and the continuum according to equations (4.13) and (4.14). The bound state achieves maximum intensity at the zone boundary where it absorbs the total weight.

Equation (4.15) may also be viewed as a sum rule connecting the dynamic to the static correlation function, namely

$$\int_0^\infty d\omega\, G^{zz}(k, \omega) = \frac{1}{\Lambda}\sum_{mn} \exp[ik(m-n)]\, \langle\Omega|S_m^z S_n^z|\Omega\rangle. \tag{4.16}$$

The latter can be computed more directly by using in the right-hand side of equation (4.16) the leading-order strong-coupling approximation to the ground state given earlier in equation (3.2). A short calculation reproduces the result in equation (4.15), thus providing an important check of consistency. One should finally note that the semiclassical result (2.8) also satisfies the sum rule (4.15).

The picture of the longitudinal correlation function described above suggests that the $e\bar{e}$ bound state should be observable in neutron scattering through out-of-plane fluctuations. In particular, the bound state should be conspicuous for crystal momenta near the zone boundary where it achieves maximum intensity. For $|k| < k_0$ a δ-function peak ceases to exist, but figure 4 indicates that a relatively sharp peak of lower intensity continues to appear at frequency $\Omega_k^{\max}$ given by equation (4.11). Hence in figure 5 we plot the bound-state dispersion using $\Omega_k^{e\bar{e}}$ of equation (4.10*b*) for $|k| > k_0$ (full curve) and $\Omega_k^{\max}$ of equation (4.11) for $|k| < k_0$ (broken curve). Note that the two curves join smoothly at $|k| = k_0$. For comparison, the (anti)exciton mode is also displayed in figure 5. We thus see that the dispersion of the $e\bar{e}$ bound state exhibits the general characteristics of the dispersion of the mirror mode observed in the experiment in [8], except for some apparent quantitative differences near the zone centre. These differences are probably

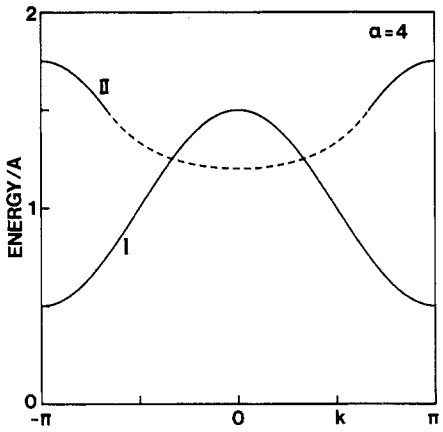

Figure 5. Comparison of the energy–momentum dispersion of the (anti)exciton mode (curve I) with that of the e$\bar{e}$ bound state (curve II) for a typical intermediate coupling ($a = 4$) and antiferromagnetic exchange interaction ($\delta = -1$). that of the e$\bar{e}$ bound state (curve II) for a typical explained in the text.

not crucial in view of the fact that the intensity of out-of-plane fluctuations is vanishingly small near the zone centre. Of course, it is still possible that the observed mirror mode is due to couplings that go beyond the simple Hamiltonian (1.1). Nonetheless, to the extent that this simple model is relevant for $CsFeBr_3$, our calculation strongly suggests that an e$\bar{e}$ bound state is present in out-of-plane fluctuations and must be resolved before other explanations of the mirror mode are contemplated.

We conclude this section with a word of caution concerning a consistent use of the derived approximate expressions for the dynamic correlation functions. For intermediate anisotropies of actual interest, the transverse function (4.3) is much more accurate than the longitudinal function (4.10), because the latter was computed only to leading order in the strong-coupling expansion. Therefore, if the parameters of the model are extracted from equation (4.3), it would be inconsistent to use them directly for the analysis of out-of-plane fluctuations through equations (4.10). An example is given in figure 5 which compares the dispersion of the (anti)exciton mode with that of the e$\bar{e}$ bound state, for a typical intermediate coupling ($a = 4$) and isotropic antiferromagnetic exchange interaction ($\delta = -1$). The (anti)exciton dispersion is then given by equation (4.4) which is an accurate expression for both strong and intermediate couplings, as discussed in section 3. However, in figure 5, we actually use equation (4.4) only to leading order, i.e. $\omega_k \simeq A[1 + (2\cos k)/a]$, to be consistent with the corresponding leading-order calculation of the dispersion of the e$\bar{e}$ bound state given in equations (4.10). Therefore, for a consistent analysis of out-of-plane fluctuations, equations (4.10) should be used in conjunction with parameters extracted from the transverse function (4.3) truncated to leading order. Of course, a more satisfactory procedure would be to calculate higher-order corrections to equations (4.10); but these appear difficult to obtain because of the inherent degenerate perturbation theory.

5. Concluding remarks

We have developed a reasonably complete theoretical framework for quantum spin-1 chains with strong planar anisotropy, using both semiclassical and strong-coupling methods. We have shown that more reliable results are obtained with a direct strong-coupling expansion. These results are summarised by the explicit expressions for the

dynamic correlation functions given in equations (4.3) and (4.10), which should prove useful for a detailed analysis of neutron scattering experiments.

Although the strong-coupling expansion was shown to be superior to the $1/n$ expansion in the present problem, one should not hasten to generalise such a conclusion. In fact the $1/n$ expansion is a more flexible framework and can prove useful in a variety of problems for which the standard semiclassical theory of magnetism fails. For instance, the $1/n$ expansion yields useful information for the weak-coupling region of the present model [4], for quantum spin-1 systems with competing quadratic and biquadratic interactions [5], for the currently popular t–J model [13], and so on.

Acknowledgments

This work was supported in part by a research grant from the EEC (ESPRIT-3041) and by the US Department of Energy.

Note. One of the referees made the observation that, if one uses for the exciton dispersion the simple functional form (2.3) with renormalised parameters, namely

$$\omega_k = A'[1 - (4\cos k)/a']^{1/2} \tag{1}$$

with $A' = A(1 + 3/a^2)$ and $a' = a(1 + 3/a^2)$, the results of the strong-coupling expansion (3.6) are reproduced to second order. Although the δ-term in the third-order correction to the dispersion (3.6) and in the second-order correction to the intensity (4.3) cannot be accounted for by a similar renormalisation, this observation is of some importance because experiments on $CsFeBr_3$ have thus far been analysed essentially on the basis of (1). Using as input the experimental value $a' = 4.7$ one finds that $a = 3.9$, which is significantly larger than the value $a = 3.3$ obtained in the text. The difference is due partly to the limited expansion and partly to the additional δ-term in (3.6). However, it is an indication that the third-order correction in (3.6), which captures some of the subtleties of out-of-plane fluctuations, is significant in this region of intermediate couplings. Needless to say, out-of-plane fluctuations become crucial in the calculation of both exciton bound states and the longitudinal correlation function (4.10) which are the main new results of the present work that were not anticipated by earlier treatments [10].

References

[1] Bethe H A 1931 *Z. Phys.* **71** 205
[2] Steiner M, Villain J and Windsor C G 1976 *Adv. Phys.* **25** 87
[3] Muller G, Thomas H, Beck H and Bonner J C 1981 *Phys. Rev.* B **24** 1429
[4] Papanicolaou N 1984 *Nucl. Phys.* B **240** 281; 1985 *Z. Phys.* B **61** 159
[5] Papanicolaou N 1988 *Nucl. Phys.* B **305** 386
[6] Papanicolaou N and Spathis P 1989 *J. Phys.: Condens. Matter* **1** 5555
[7] Steiner M, Kakurai K, Knop W, Dorner B, Pynn R, Hapek U, Day P and McLeen G 1981 *Solid State Commun.* **38** 1179
[8] Dorner B, Visser D, Steigenberger U, Kakurai K and Steiner M 1988 *Z. Phys.* B **72** 487
[9] Dorner B, Visser D, Steigenberger U, Kakurai K and Steiner M 1989 *Physica* B **156** 263
[10] Lindgard P A 1983 *Physica* B **120** 190
[11] Orbach R 1958 *Phys. Rev.* **112** 309
[12] Papanicolaou N and Psaltakis G C 1987 *Phys. Rev.* B **35** 342
[13] Marder M, Papanicolaou N and Psaltakis G C 1990 *Phys. Rev.* B **41** 6920